RSC Advances

ROYAL SOCIETY OF CHEMISTRY

www.rsc.org/advances

RSC Advances

COMMUNICATION

3-D N-doped porous graphene-like network and vanadium nitride co-promoted Pt electrocatalyst with high activity and stability for the oxygen reduction reaction

Received 00th January 20xx,
Accepted 00th January 20xx

DOI: 10.1039/x0xx00000x

Zesheng Li,*[a] Bolin Li,[a] Zhishen Liu,[a] Zhenghui Liu[a] and Dehao Li[a]

Three dimensional (3D) N-doped porous graphene and vanadium nitride co-promoted Pt (3DNPG/VN/Pt) electrocatalyst was first presented in this work. Such multi-component catalysts exhibited superior performances for the oxygen reduction reaction (ORR). The mass activity of 3DNPG/VN/Pt is up to 535 mA mg^{-1} Pt (after IR correction), which is 4.35 times as high as that of commercial Pt/C (123 mA mg^{-1} Pt). Higher stability of the 3DNPG/VN/Pt is also demonstrated by comparison to the commercial Pt/C.

Multiple hybrid nanostructured materials often give rise to many extraordinary collective and synergic properties not present in the individual counterparts, leading to potential applications of these hybrid architectures in diverse electrochemical fields.[1] Considerable research efforts made on multiple hybrid nanostructures have recently been focused on the electrocatalysis applications.[2] The development of multi-component catalysts offers great promise to tangibly enhance catalytic performances and reduce material cost for the commercialization of fuel cells.[3]

Previous literatures have indicated that one of the desirable architectures for such hybrid catalysts is the metal carbide-based synergetic platinum (Pt) catalysts: e.g., Pt/WC/C[4], Pt/MoC/C[5], and Pt/VC/C[6] systems. Among these hybrid structures, metal carbides are widely recognized as the synergetic components imparting improved catalytic activity and long-term stability for the catalyst systems.[7] On the other hand, developing graphene-based hybrid catalysts is an effective route to increase the activity of platinum catalysts due to the notable promoted effects of graphene.[8] With this in mind, the combination of carbide and graphene has become an alternative strategy for designing high performance Pt-based electrocatalyst for the application in fuel cells.

Recently, metal nitrides were found to be the promising active and synergetic catalysis materials for fuel cells due to their highly electronic conductivity, well thermal stability and electrochemical stability in fuel cell operating conditions.[9] For example, Pt/TiN/C,[10] Pt/WN/C[11] and Pt/MoN/C[12] as electrocatalysts in fuel cells has been reported, which showed higher catalytic activity and better stability than those of metal carbide-based electrocatalysts. On the other hand, N-doped graphene was also reported to be an attractive active and synergetic component for the Pt-based electrocatalyst owing to the larger surface area, high electric conductivity, and nitrogen-related active sites.[13] Particularly, the hybrid architecture composed of metal nitrides and Pt metal, directly grown on the N-doped graphene, would be a promising electrocatalyst with greatly improved catalytic performances for fuel cells, depending on the co-promoted effects from the dual synergetic components.

For the oxygen reduction reaction (ORR) electrode of fuel cells, several technical parameters are especially significant, for instance, the oxygen diffusion and water removal. It is widely believed that the mass-transport loss, incurred by the poor oxygen-transport through the electrode layer and diffusion medium is a fundamental contribution to the voltage loss for fuel cells.[14] Therefore, a highly poriferous framework for the ORR electrode is absolutely essential for the manufacturing of high-performance fuel cells.[15] The newly developed three-dimensional (3D) graphene-like (ultrathin graphite nanosheets) porous networks[16] are highly expected to meet the above requirements for high-efficiency mass transport, due to their favorable 3D networks and sufficient macroporous structures.

Herein, we propose the novel 3D N-doped porous graphene-like networks (3DNPG) with abundant mesopores and macropores, for the construction of an efficient metal nitride (vanadium nitride, VN) synergeticly enhanced Pt electrocatalyst for the ORR of fuel cells. The 3DNPG/VN/Pt hybrid electrocatalyst are designed on the basis of the following considerations: (i) the 3-D macroporous networks enable fast mass-transport kinetics of the system, (ii) the abundant mesoporous structures can accommodate and steadily anchor the VN an Pt nanoparticles, (iii) the nitrogen-related active sites of N-doped graphene and VN can provide co-promoted effects towards the Pt electrocatalyst. With these merits, we demonstrate that ORR electrocatalysts with high performances can be designed on the basis of this novel hybrid nanostructured material.

[a] *Development Center of Technology for Petrochemical Pollution Control and Cleaner Production of Guangdong Universitites, College of Chemical Engineering, Guangdong university of Petrochemical Technology, Maoming, Guangdong, 525000, China.*

Corresponding authors
E-mail addresses: Zesheng Li, lzs212@163.com*

† Footnotes relating to the title and/or authors should appear here.
Electronic Supplementary Information (ESI) available: [details of any supplementary information available should be included here]. See DOI: 10.1039/x0xx00000x

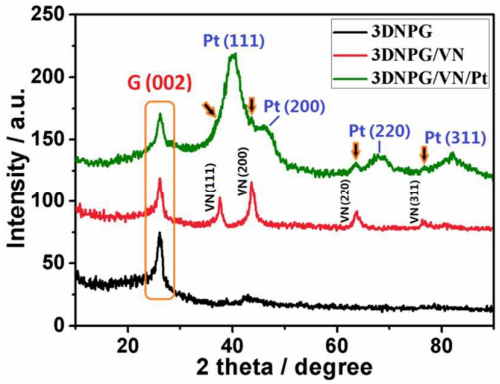

Fig. 1 XRD patterns of the 3DNPG, 3DNPG/VN and 3DNPG/VN/Pt samples.

For the synthesis of 3DNPG support, an activation/graphitization synchronous strategy is used with ion-exchange resin carbon source and melamine as nitrogen source. The 3DNPG/VN is synthesized by the one-step sintering of 3DNPG with NH_4VO_3 and melamine. The 3DNPG/VN/Pt is synthesized by the Intermittent Microwave Heating (IMH) method. More experimental details are provided in the ESI. X-ray diffraction (XRD) patterns of as-prepared samples are shown in Fig. 1. All these samples indicate similar graphitic (G) (002) peaks of 3DNPG at 26.2°, indicating the well crystalline structures of the graphene-like product. For the 3DNPG/VN, a series of diffraction peaks at 37.6°, 43.7°, 63.6° and 76.3° are observed, corresponding to the 111, 200, 220 and 311 planes of VN phase (JCPDS, 65-5288). The average crystallite size of VN crystals calculated by Scherrer equation is about 9.3 nm from the 111 crystal plane. For the 3DNPG/VN/Pt, the new diffraction peaks at 40.1°, 46.3°, 67.9° and 81.6° correspond to the (111), (200), (220) and (311) planes of Pt phase (JCPDS, 65-2868). The average crystallite size of Pt crystals is calculated to be about 2.1 nm from the 111 crystal plane. The diffraction peaks of VN phase (marked by arrows) can be observed in 3DNPG/VN/Pt, which indicates that the hybrid architecture of VN and Pt grown on 3DNPG has been successfully synthesized.

Fig. 2 displays the typical scanning electron microscopy (SEM) images of the 3DNPG sample, indicating the formation of a well-defined 3D macroporous network architecture that is made up of numerous interconnected graphene-like nanosheets. The diameter of these macropores ranges from 300 to 500 nm. The thickness of nanosheets is less than 20 nm. On the other hand, the transmission electron microscopy (TEM) images (Fig. 3) further demonstrate the fascinating 3D configuration, which is constituted of ultrathin (15 nm) and interlaced nanosheets (Fig. 3 A and B). The formation of mesopores (2-10 nm, marked by arrows) on these nanosheets was confirmed by the higher-magnification TEM image (Fig. 3 C). And a high-resolution (HR) TEM image (Fig. 3 D) gives a precise description of the mesoporous texture, where the legible crystal lattice belong to the graphitic basal plane unit (sp^2-bonded carbon), and the amorphous area is originated from the porous structures and little sp^3-bonded carbon. At the same time, the nitrogen adsorption-desorption analysis of 3DNPG sample (Fig. S1 A) exhibits the typical characteristics of mesoporous materials, with increasing adsorption volume and pronounced desorption hysteresis loops. The pore size distribution (Fig. S1 B) indicates that the sample has the satisfactory mesopores (2-10 nm) and remarkable macropores (50-300 nm). The BET surface area of 3DNPG sample is 1065 $m^2 g^{-1}$.

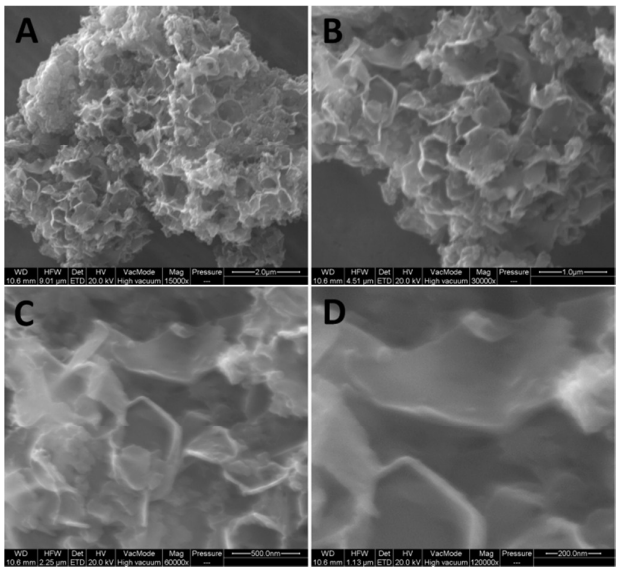

Fig. 2 Typical SEM images the 3DNPG sample in different magnifications.

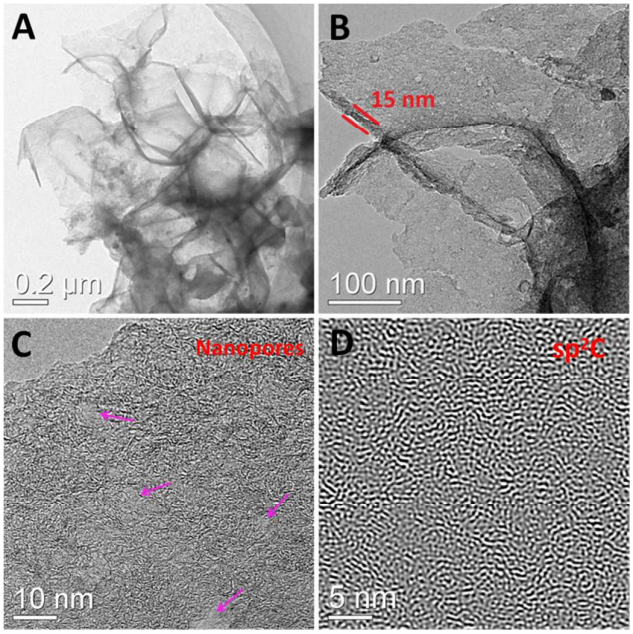

Fig. 3 Typical TEM images the 3DNPG sample in different magnifications.

Fig. 4 shows the typical TEM images of the 3DNPG/VN/Pt sample. From the low magnification images (Fig. 4 A and B), it can be seen that innumerable nanoparticles are well dispersed on the 3DNPG. A higher-magnification TEM image (Fig. 4 C) clearly shows that these nanoparticles are composed of two different components, where the larger one in size of about 10 nm is the VN nanoparticles and the smaller one in size of about 2 nm is the Pt nanoparticles. The HR-TEM image (Fig. 3 D) reveals the surrounding relation between VN and Pt nanoparticles, and the existence of sp^2-bonded graphitic carbon. The result further demonstrates the successful integration of VN and Pt components on 3DNPG. The graphitic and mesoporous structures can provide a high electronic conductivity and structural stability for both the VN and Pt nanoparticles.

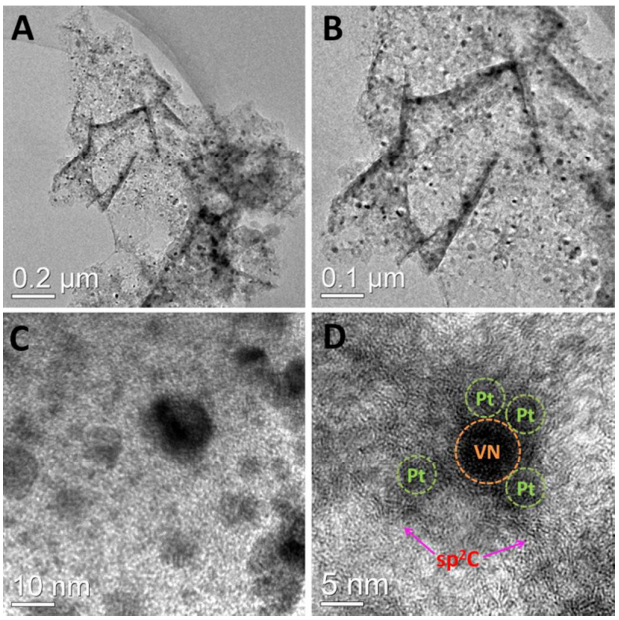

Fig. 4 Typical TEM images the 3DNPG/VN/Pt sample in different magnifications.

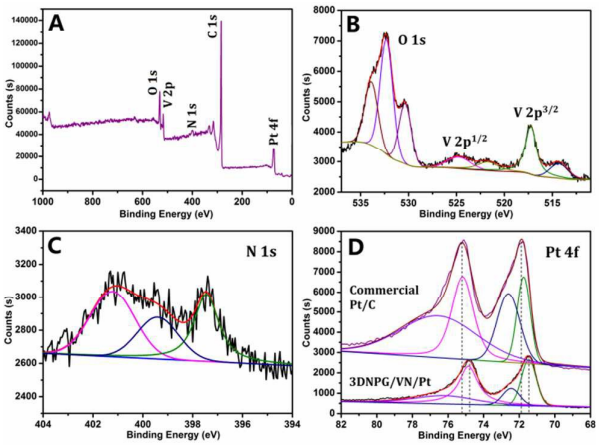

Fig. 5 XPS patterns the 3DNPG/VN/Pt sample: (A) the overall survey, (B) V 2p-O 1s, (C) N1s and (D) Pt 4f.

The X-ray Photoelectron Spectroscopy (XPS) is further applied to reveal the surface states of 3DNPG/VN/Pt catalyst, with the results shown in Fig. 5. The overall survey (Fig. 5 A) shows the sample is composed of C, O, N, V and Pt elements. Fig. 5 B displays the high-resolution XPS spectra of O 1s and V 2p, indicating the presence of an oxide layer on the surface of VN.[17] The peak at 530.4 eV of O1s can be attributed to the lattice oxygen of metal oxides on the surface of VN. The peak at 532.3 eV of O1s is mainly attributed to the oxygenated groups (e.g. C=O) on the 3DNPG. The peak at 533.8 eV of O1s belongs to the adsorbed hydroxyl oxygen (OH^-) on the surface of catalyst sample. The V $2p^{1/2}$ and V $2p^{3/2}$ peaks at 514.3 eV and 521.7 eV belong to vanadium in the VN crystalline, while the other two peaks at 517.2 eV and 524.8 eV can be assigned to oxidation states of vanadium.[18] For the N 1 s spectrum (Fig. 5 C), the peak at 397.4 eV is the typical characteristic of metal nitride (VN).[19] The peaks at 401.2 eV and 399.5 eV are generally assigned to graphitic and pyridine type N bonding to crystal structure of carbon,

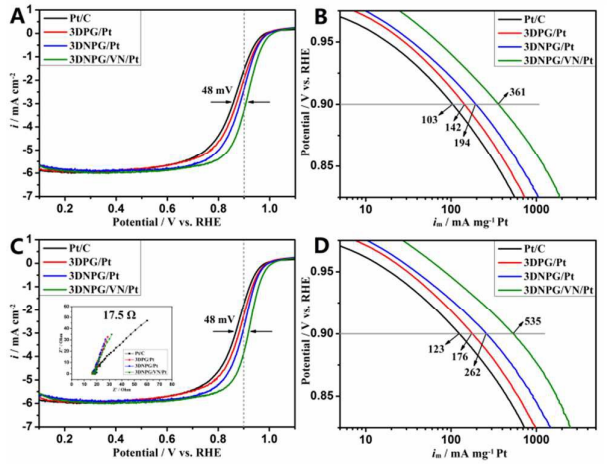

Fig. 6 Electrocatalytic performances of the samples: (A,C) overall ORR curves, (B,D) Pt mass activities at 0.9V (vs. RHE) (A,B: before IR correction; C,D: after IR correction).

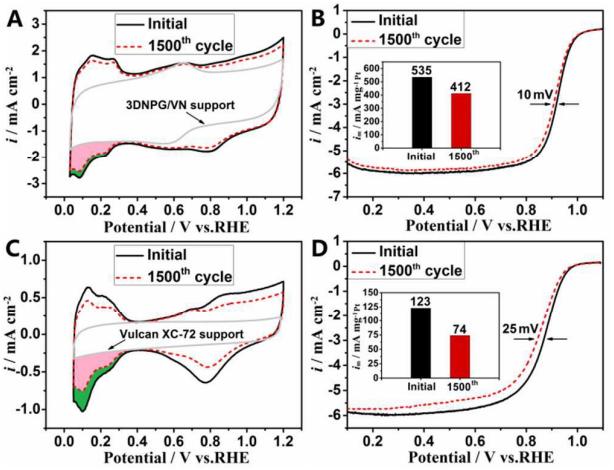

Fig. 7 Electrochemical stability of (A and B) 3DNPG/VN/Pt and (C and D) TKK Pt/C. A and C show the Cyclic voltammograms (CV) curves, and B and D show the ORR curves before and after 1500 CV cycles (the insets are the mass activities).

highly indicative of the formation of N-doped graphene materials.[13] The Pt 4f spectra of the commercial Pt/C (TKK, 47.60 % Pt) and 3DNPG/VN/Pt (14.58 % Pt) are also compared in Fig. 5 D. The 3DNPG/VN/Pt reveals about 0.5 eV decrease in binding energy compared to that of the commercial Pt/C, which is mainly due to the electron transfer from VN to metallic Pt (i.e. the occurring of electron-donating effect [20]), suggesting that the hybrid catalyst is catalytically more active than the single Pt catalyst.

The ORR electrocatalytic performances of the samples are further demonstrated in Fig. 6. The comparative ORR measurement of the samples, including the Pt/C, 3DPG/Pt, 3DNPG/Pt and 3DNPG/VN/Pt (based on the same weight of Pt) have been carried out, in order to demonstrate the co-promoted effects from N-doped graphene and VN. The ORR polarization curves (see Fig. 6A) were recorded at 25 ^oC in an O_2-saturated 0.1 M $HClO_4$ solution with a sweep rate of 5 mV/s and a rotation speed of 1600 rpm. The ORR onset potential of Pt/C, 3DPG/Pt, 3DNPG/Pt and 3DNPG/VN/Pt are 0.983, 0.992, 1.005 and 1.018 V, respectively. And the half-potential ($E_{1/2}$) value of the 3DNPG/VN/Pt is about 48 mV more positive than that of the Pt/C,

which suggests that the intervention of 3DNPG and VN components can reduce the overpotential of ORR evidently.

The mass activities of the Pt-based catalyst were calculated from the ORR data by using the mass transport correction for a rotating disk electrode[21]: $i_k=i_d i/(i_d-i)$, where i is the experimentally obtained current, i_d refers to the measured diffusion-limited current and i_k the mass-transport-free kinetic current. The Pt mass activities at 0.9 V are calculated to be about 103, 142, 194 and 361 mA mg^{-1} Pt, for Pt/C, 3DPG/Pt, 3DNPG/Pt and 3DNPG/VN/Pt, respectively (see Fig. 6B). Obviously, 3DNPG/Pt shows higher mass activity (194 mA mg^{-1} Pt) than that of 3DPG/Pt (142 mA mg^{-1} Pt), which demonstrates that the nitrogen-related active sites of N-doped graphene give beneficial effect for Pt metal. Furthermore, 3DNPG/VN/Pt shows much higher (361 mA mg^{-1} Pt) mass activity than that of 3DNPG/Pt (194 mA mg^{-1} Pt), which reveals a more remarkable promoted effect on Pt metal from VN component. Owing to the co-promoted effects from N-doped graphene and VN, the Pt mass activity of 3DNPG/VN/Pt is about 3.5 times as high as that of Pt/C.

It is well known that the "IR correction" is very important for ORR measurements and the proper current values correction for Ohmic resistance should be applied.[22] In this case, the Ohmic resistance in 0.1M $HClO_4$ aqueous solution is tested to be about 17.5 Ω via the electrochemical impedance spectroscopy (see the inset in Fig. 6 C). It can be seen from Fig. 6 C that, after the IR correction, these ORR curves from 0.8 V to 1.0 V become more vertical, indicating that the improvement of ORR kinetics. After the IR correction, the Pt mass activities at 0.9 V are calculated to be about 123, 176, 262 and 535 mA mg^{-1} Pt, for Pt/C, 3DPG/Pt, 3DNPG/Pt and 3DNPG/VN/Pt, respectively (see Fig. 6D). It is worth mentioning that the Pt mass activity of 3DNPG/VN/Pt is about 4.35 times as high as that of Pt/C after the IR correction. Remarkably, in this case, the Pt-mass activity of the 3DNPG/VN/Pt has exceeded the DOE target in 2017 (440 mA mg^{-1} Pt).[23]

The electrochemical stability of both 3DNPG/VN/Pt and Pt/C electrocatalysts have been investigated by the continuous potential cycling between 0.6 and 1.2 V with a scan rate of 50 mV/s for 1500 cycles (Fig. 7). The CV curves were obtained at 50 mV/s in N_2-saturated 0.1 M $HClO_4$ aqueous solution, and the ORR curves were obtained at 5 mV/s in O_2-saturated 0.1 M $HClO_4$ aqueous solution. The electrochemical active surface area (EASA) of the Pt-based electrocatalyst is achieved based on the integrated charge in the hydrogen adsorption peak area (as shown by the shadow in Fig. 7A and C). Before 1500 cycles, the ECSAs of the 3DNPG/VN/Pt and Pt/C electrocatalysts were 124.3 and 78.6 m^2/g, respectively. It can be deduced that the high ECSA value of 3DNPG/VN/Pt is closely correlated with the small particle size of Pt (as determined by TEM). And the integration of VN and Pt may be good for the high ECSA value of Pt, where further examination is needed. After 1500 cycles, the ECSAs of the 3DNPG/VN/Pt and Pt/C electrocatalysts were 111.6 and 51.2 m^2/g, respectively. Obviously, the 3DNPG/VN/Pt maintains higher ECSA retention of about 87 %, while that of Pt/C is only 65 % after 1500 time continuous potential cycles. Only 10 mV degradation in the half-wave potential for 3DNPG/VN/Pt (Fig. 7B), while that of Pt/C is 25 mV (Fig. 7D). Remarkably, a relatively higher Pt mass activity of 412 mA mg^{-1} Pt can be obtained for 3DNPG/VN/Pt after 1500 cycles, while that of Pt/C is only 74 mA mg^{-1}. The less loss of the active surface area and higher ORR activity indicate that the electrochemical stability of the 3DNPG/VN/Pt hybrid electrocatalyst is better than that of the commercial Pt/C electrocatalyst.

In summary, this study demonstrates the first synthesis of newly ternary 3DNPG/VN/Pt hybrid architectures with unique 3D network configuration. The nitrogen-related active sites of 3DNPG and VN provide remarkable co-promoted effects towards the Pt metal. The Pt mass activity of 3DNPG/VN/Pt electrocatalyst for the ORR is up to 535 mA mg^{-1} Pt (after IR correction), which is much higher than that of commercial Pt/C (123 mA mg^{-1} Pt) at 0.9 V. Expressly, the favourable mesoporous structures of 3DNPG endow with excellent structural stability of the hybrid electrocatalyst. It is expected that the constructing of hybrid architecture with 3-D N-doped porous graphene-like network and metal nitrides is a promising strategy to build high-performance Pt-based electrocatalysts with a superior activity and desirable stability for the ORR application.

Acknowledgements

Financial support by the National Natural Science Foundation of China (21443006), Provincial Natural Science Foundation of Guangdong (2014A030310179), Young Creative Talents Project of Guangdong Province Education Department (2014KQNCX200), Science and Technology Project of Maoming (2014006) and Doctor Startup Project of local University (513086) are gratefully acknowledged.

Notes and references

1 (a) M. Christopher Orilall, U. Wiesner, *Chem. Soc. Rev.*, 2011, **40**, 520-535. (b) H. Wang, H.J. Dai, *Chem. Soc. Rev.*, 2013, **42**, 3088-3113.

2 (a) B. Xia, Y. Yan, X. Wang, X.W. Lou, *Mater. Horiz.*, 2014, **1**, 379-399. (b) H. Huang, X. Wang, *J. Mater. Chem. A*, 2014, **2**, 6266-6291.

3 (a) Z. Zhang, J. Liu, J. Gu, L. Su, L. Cheng, *Energy Environ. Sci.*, 2014, **7**, 2535-2558. (b) S. Zhang, Y. Shao, G. Yin, Y. Lin, *J. Mater. Chem. A*, 2013, **1**, 4631-4641.

4 (a) Z. Yan, H. Meng, P.K. Shen, R. Wang, L. Wang, K. Shi, H. Fu, *J. Mater. Chem.*, 2012, **22**, 5072-5079. (b) Z. Yan, F. Li, J. Xie, X. Miu, *RSC Adv.*, 2015, **5**, 6790-6796.

5 (a) Z. Yan, G. He, P. K. Shen, Z. Luo, J. Xie, M. Chen, *J. Mater. Chem. A*, 2014, **2**, 4014-4022. (b) Z. Yan, J. Xie, P.K. Shen, *J. Power Sources*, 2015, **286**, 239-246.

6 (a) G. He, Z. Yan, X. Ma, H. Meng, P.K. Shen, C. Wang, *Nanoscale*, 2011, **3**, 3578-3582. (b) Z. Yan, L. Gao, M. Zhang, J. Xie, M. Chen, *RSC Adv.*, 2015, **5**, 9561-9564.

7 X. Ma, H. Meng, M. Cai, P.K. Shen, *J. Am. Chem. Soc.*, 2012, **134**, 1954-1957.

8 M. Liu, R. Zhang, W. Chen, *Chem. Rev.*, 2014, **114**, 5117-5160.

9 (a) S. Dong, X. Chen, X. Zhang, G. Cui, *Coordin. Chem. Rev.*, 2013, **257**, 1946-1956. (b) W. Chen, J.T. Muckermana, E. Fujita, *Chem. Commun.*, 2013, **49**, 8896-8909.

10 Z. Pan, Y. Xiao, Z. Fu, G. Zhan, S. Wu, C. Xiao, G. Hua, Z. Wei, *J. Mater. Chem. A*, 2014, **2**, 13966-13975.

11 S. Jing, L. Luo, S. Yin, F. Huang, Y. Jia, Y. Wei, Z. Sun, Y. Zhao, *Appl. Catal. B-Environ.*, 2014, **147**, 897-903.

12 Y. Xiao, Z. Fu, G. Zhan, Z. Pan, C. Xiao, S. Wu, C. Chen, G. Hua, Z. Wei, *J. Power Sources*, 2015, **273**, 33-40.

13 S. Zhao, H. Yin, L. Du, G. Yin, Z. Tang, S. Liu, *J. Mater. Chem. A*, 2014, **2**, 3719-3724. J. Zhu, M. Xiao, X. Zhao, C. Liu, J. Ge, W. Xing, *Nano Energy*, 2015, **13**, 318-326.

14 L. Cindrella, A.M. Kannan, J.F. Lin, K. Saminathan, Y. Ho, C.W. Lin, J. Wertz, *J. Power Sources*, 2009, **194**, 146-160.

15 W. Yuan, Y. Tang, X. Yang, Z. Wan, *Applied Energy*, 2012, **94**, 309-329.

16 Y. Li, Z. Li, P.K. Shen, *Adv. Mater.*, 2013, **25**, 2474-2480.

17 K. Huang, K. Bi, C. Liang, S. Lin, R. Zhang, W.J. Wang H.L. Tang, M. Lei, *Scientific reports*, 2015, **5**.

18 X. Lu, M. Yu, T. Zhai, G. Wang, S. Xie, T. Liu, C. Liang, Y. Tong, Y. Li, *Nano Lett.*, 2013, **13**, 2628-2633.

19 A.M. Glushenkov, D. Hulicova-Jurcakova, D. Llewellyn, G.Q. Lu, Y. Chen, *Chem. Mater.*, 2010, **22**, 914-921.

20 Z. Li, S. Ji, B.G. Pollet, P.K. Shen, *Chem. Commun.*, 2014, **50**, 566-568.

21 K Mayrhofer, D. Strmcnik, B. Blizanac, V. Stamenkovic, M. Arenz, N. Markovic, *Electrochim. Acta*, 2008, **53**, 3181-3188.

22 D. Van der Vliet, D. Strmcnika, C. Wang, V. Stamenkovic, N. Markovic, M. Koper, *J. Electroanal. Chem.*, 2010, **647**, 29-34.

23 U. S. Department of Energy, Technical Plan: Fuel Cells, 2011, http://www1.eere.energy.gov/hydrogenandfuelcells/mypp/pdfs/fuel_cells.pdf.